J. Water Environ. Nanotechnol., 5(3): 283-293 Summer 2020

ORIGINAL RESEARCH PAPER

Green Synthesis of Magnesium Oxide Nanoparticles in MFI Type Zeolite and Its Application As a Photocatalyst

Azita Albouyeh, Afshin Pourahmad*, Hassan Kefayati

Department of Chemistry, Faculty of Science, Rasht Branch, Islamic Azad University, Rasht, Iran

Received: 2020-05-12 Accepted: 2020-06-15 Published: 2020-08-01

ABSTRACT

Rice husk silica (RHS), an agriculture waste, was used as a silica source for MFI zeolite synthesis. Magnesium oxide (MgO) nanoparticles (NPs) were grown in zeolite substrates using a solid-state reaction. The synthesized nanocomposite (NC) was characterized by X-ray diffraction (XRD), scanning electron microscopy (SEM), diffuse reflectance spectroscopy (DRS), and transmission electron microscopy (TEM) techniques. The BET results demonstrated that the specific surface area of MgO/RHS-MFI NC was smaller than RHS-MFI zeolite. Magnesium oxide NP was found capable of being encapsulated into pores of RHS-MFI zeolite. This research's most principal objective was the evaluation of the photocatalytic process capability of MgO/RHS-MFI zeolite heterogeneous nanocomposite over methylene blue (MB) dye. Results showed that the MB degradation reached 80 % under UV light at pH=9. RHS-MFI affected the photocatalytic activity of magnesium oxide due to the decrease in the recombination rate of the electron-hole in magnesium oxide semiconductor. A plausible oxidation mechanism was also proposed.

Keywords: *Environmental Nanotechnology, Green chemistry, Pollution, Rice husk silica*

How to cite this article

Albouyeh A., Pourahmad A., Kefayati H. Green Synthesis of Magnesium Oxide Nanoparticles in MFI Type Zeolite and Its Application As a Photocatalyst. J. Water Environ. Nanotechnol., 2020; 5(3): 283-293.

DOI: 10.22090/jwent.2020.03.008

INTRODUCTION

Synthetic dyes are used on a large scale and are extremely soluble and stable in water. These dyes are found in the wastewater of many industries such as petroleum, cosmetics, printing, and textile, in which enormous amounts of toxic waste are generated [1, 2]. Dyes affect human health remarkably since they do not decompose biologically; Hence the removal of toxic dyes from industrial wastewater before unloading them into the environment by cheap and eco-friendly adsorbents is becoming more important from the toxicological and ecological point of view. Heterogeneous photo-oxidation is a low-cost and efficient method for detoxifying organic dye molecules. Photocatalysis materials using low energy photon adsorption act as the producers of oxidant radicals and would keep down the material application and the treatment cost due to the catalyst recycling [3]. A quick rate of technological progress requires the usage of advanced and innovative products. The micrometric and nanometric materials that have expanded over recent years have become new materials for the development of innovative solutions. Magnesium hydroxide and magnesium oxide could be one of these materials. Mg(OH)2 and MgO are materials with special properties, a broad range of opportunities which cause them to be used in all practical applications. Usually, magnesium oxide is synthesized by the following procedures: precipitation, solvothermal and hydrothermal, microwave, electrochemical, and sol-gel method [4, 5]. During the past years, various semiconductors such as silver compounds, TiO_2, ZnO, CdS, and ZnS have been used as photocatalyst materials in the oxidative degradation of several synthetic dyes [6-9]; However, magnesium oxide NPs has been presented as a favored semiconductor, due to its inimitable

* Corresponding Author Email: *pourahmad@iaurasht.ac.ir*
afshinpourahmad@yahoo.com

chemical and mechanical characteristics such as high surface area, stability, cheap prize, and non-toxicity [10]. High surface area is one of the important factors for photocatalysts but, weak adsorption properties of magnesium oxide due to its low surface area have limited its oxidative applications. To overcome this restriction one has to incorporate an appropriate porous matrix into the magnesium oxide catalyst or each semiconductor with low surface area to correct its adsorptive ability [11]. Such as other NPs, magnesium oxide NPs indicated a strong inclination to agglomeration. These processes in NPs decrease their surface photocatalytic activities and dispersion stability. Therefore, incorporating or impregnation of these catalysts into the porous supporting compounds have been proposed as a very promising method. In this study, rice husk was combusted at 700 ˚C for the production of amorphous silica. The resulted amorphous rice husk silica (RHS) was then utilized as a starting material for the synthesis of MFI type zeolite. Here we describe the template synthesis of MgO NPs in RHS-MFI zeolite by solid-state reaction and ion exchange methods. The synthesized MgO/RHS-MFI nanocomposites (NCs) were characterized using XRD, EDX, and TEM. The photocatalytic activity of the prepared MgO/RHS-MFI NC was examined using photocatalytic degradation of methylene blue (MB) in water under UV light irradiation.

EXPERIMENTAL METHODS

Materials

Amorphous RHS, pellets of sodium hydroxide (Merck), tetrapropylammonium bromide (TPABr) (fluka), sodium aluminate (55–45 % Al_2O_3–Na_2O) (fluka), $Mg(NO_3)_2.6H_2O$ (Merck) and distilled water were used as starting materials in the initial mixtures for the synthesis of MFI type zeolite, and nanocomposites.

Preparation of RHS

About 30.0 g of clean rice husk (RH) was stirred with 750 mL of 1.0 mol L^{-1} HNO_3 at room temperature for 24 h. Acid treated RH was washed with a copious amount of distilled water to constant pH, dried in an oven at 100 ˚C for 24 h, and burned in a muffle furnace at 700 ˚C for 6 h to obtain white RHS.

Preparation of MFI zeolite

The synthesis was carried out using the molar composition of the starting materials, $12NaOH:30SiO_2:1Al_2O_3:6TPABr:1800H_2O$, in accordance with the previous report [12]. Amorphous RHS (1.5 g) was added to an alkali solution of NaOH (0.28 g) in distilled water. An aqueous solution of TPABr (1.23 g) and sodium aluminate (0.14 g) in distilled water was added to the RHS solution, and the whole system was placed in a stainless steel autoclave. The autoclave was heated at 150 ˚C for 1 day while the mixture was under stirring. Subsequently, the autoclave was quenched with water to achieve room temperature to interrupt the crystallization. The reaction mixture was then centrifuged and the product was washed several times with distilled water and dried at 110 ˚C for 24 h. The obtained material was then calcined at 550 ˚C for 6 h to remove the organic template.

Preparation of magnesium oxide by solid-state reaction

The magnesium-containing photocatalysts were prepared by a solid-state reaction of 0.5 g of zeolite with the amount 0.586 g of $Mg(NO_3)_2.6H_2O$. After mixing, the solid phase samples were calcined in airflow at 300 and 500 ˚C for 5 h.

Preparation of magnesium oxide by ion-exchange method

As precursors of magnesium oxide semiconductors, $Mg(NO_3)_2.6H_2O$ (0.1 mol L^{-1}) solution was prepared. To 100 mL of $Mg(NO_3)_2.6H_2O$ solution, 0.5 g of zeolite powder was added and stirred for 5 h at 25 ˚C. The sample was then washed to remove the nonexchanged and air-dried Mg^{2+}. Subsequently, the samples were calcined in airflow at 300 and 500 ˚C for 5 h.

Preparation of magnesium oxide NPs

The synthesis process of magnesium oxide NPs was performed using the sol-gel method [13]. First, 50 g of $MgCl_2{\cdot}6H_2O$ was added to a 1L beaker containing 250 mL distilled water, followed by the addition of 25 mL 1 N NaOH solution. This process is followed by 3hours of rapid stirring to form white precipitates. The suspension centrifugation was carried out during 6 mins at 2500 rpm to obtain $Mg(OH)_2$ gel and then rinsed using distilled water for several times to achieve the impurities removal. Afterward, the product was dried at 60 ˚C for 24 h and calcined at 450 ˚C for 3 h in a furnace in an attempt to get magnesium oxide nanoparticles.

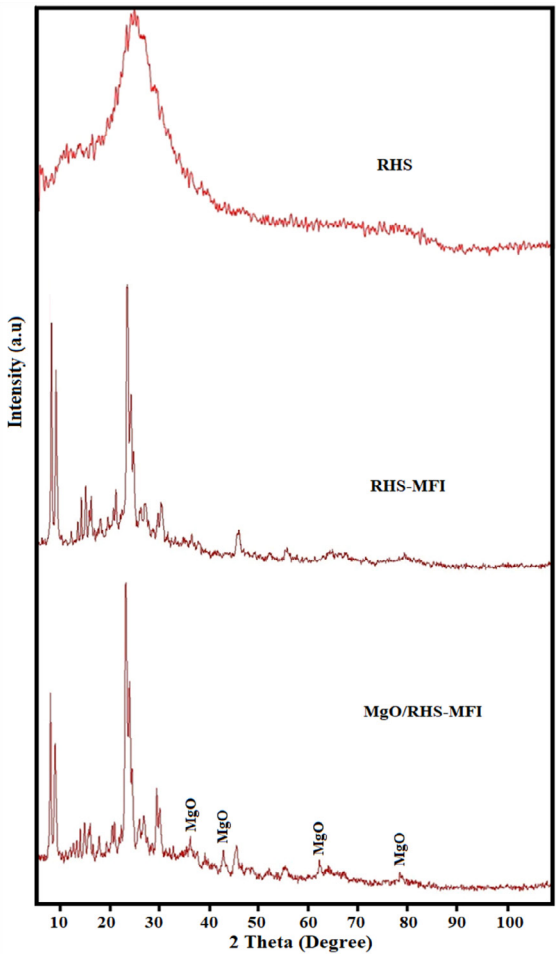

Fig. 1. XRD patterns of samples

Evaluation of photocatalytic activity

The photocatalytic activities of the MgO/RHS-MFI photocatalyst, MGO, and RHS-MFI samples were evaluated via decomposing MB dye solution at room temperature. The concentration of MB and photocatalyst were set as 20 mg/L and 0.09 g/L, respectively. The photocatalytic degradation process was observed by the change of the absorbance maximum in the optical absorption spectra of MB dye (λ_{max} ~ 664 nm). Prior to irradiation, the suspensions were magnetically stirred in the dark for 20 mins to establish adsorption or a desorption equilibrium. The dispersions were kept under constant air-equilibrated conditions before and during irradiation. A125 W Hg-lamp with maximum emission at approximately 313.2 nm was employed as an irradiation source (UV light) and located 10 cm above the reactor to trigger the photocatalytic reaction.

Characterization

X-ray diffraction (XRD) pattern was recorded on a Seisert Argon 3003 PTC using nickel-filtered XD-3a CuKa radiations (λ=1.5418˚A). The UV-vis diffused reflectance spectra (UV-vis DRS) were obtained from UV-vis Scinco 4100 spectrometer with an integrating sphere reflectance accessory. BaSO4 was used as reference material. UV-vis absorption spectra were recorded using a Shimadzu 1600 pc in the spectral range of 190–900 nm. Transmission electron microscopy (TEM) was performed on a Philips CM10 and microscope operated at 100 kV. Samples were prepared by dispersing the powder in ethanol. Imaging was enabled by depositing few drops of suspension on a carbon-coated 400-mesh Cu grid. The solvent was left to evaporate before imaging. The specific surface area and pore volume of the samples were calculated according to the Brunauer-Emmett-Teller (BET) method.

RESULTS AND DISCUSSION

Characterization of magnesium oxide NPs in MFI zeolite

The powder XRD pattern of the RHS, RHS-MFI, and MgO/RHS-MFI samples are presented in Fig. 1. A broad peak at 2θ value of 17–24° related to amorphous silica (RHS) structure is also observed [14].

The XRD profile of RHS-MFI zeolite was matched quite well with the pattern given in the literature [12] which allowed up identifying the product as MFI zeolite. The XRD patterns show peaks at 2θ = 8 °, 8.9°, 23.2 °, 23.9 °, 24.4° which correspond to the specific peaks of MFI zeolite. This indicates that the synthesized RHS-MFI zeolite powders are MFI zeolite crystals [15]. The XRD patterns of MgO/RHS-MFI NC (synthesized by solid-state reaction method at 300 ˚C) not only show peaks related to MFI zeolite, but also indicate additional peaks at 2θ= 36.2, 42.9, 62.37, and 78.74° corresponding to (111), (200), (220), and (222) planes of the Face Centered Cubic (FCC) structured magnesium oxide NPs with a space group of Fm-3m (JCPDS file no. 89-7746) [16]. No other peaks were detected in the XRD pattern confirming the high purity of the obtained magnesium oxide NPs. The average crystallite size ranging from 29 nm was estimated by using Scherrer's formula. The MgO/RHS-MFI NC was synthesized by both methods, solid-state reaction at 500 ˚C and ion exchange. However, the XRD results showed that by solid-state method at 500 ˚C, the X-ray diffraction pattern of magnesium oxide NPs was very weak in the nanocomposite but for ion exchange method no peaks were found for MgO NPs.

Fig. 2 shows SEM micrographs of RHS derived from a rice husk, RHS-MFI, and MgO/RHS-MFI NC. SEM image of RHS indicated the outer epidermis of synthesized SiO_2 is well organized and has a corrugated structure. The SEM image of synthesized RHS was similar to rice husk; due to during calcination, only organic compounds in rice husk were removed. The morphologies of the RHS-MFI and MgO/RHS-MFI samples showed greater similarity to each other, taking the form of large rounded aggregates (uniform size with a diameter of about 450 nm). RHS-MFI was composed of single-crystal nanoparticles with diameters of 45-50 nm that increased in size (50-60 nm) with incorporating MgO NPs in zeolite.

The RHS and MgO/RHS-MFI samples were characterized by TEM. Fig. 3A showed that the samples possessed a highly heterogeneous morphology. The TEM image of MgO/RHS-MFI indicates two-color parts. The light part related to the RHS-MFI section and the dark part is MgO nanoparticles that are aggregated into zeolite. Fig. 3B indicates the elemental mapping of MgO/RHS-MFI sample. The result shows that there are all elements Al, Si, O, and Mg in NC.

The optical properties of MgO NPs and MgO/RHS-MFI that have been recorded by the UV–visible diffuse reflectance spectra are shown in Fig. 4. The MgO and MgO/RHS-MFI nanocomposites exhibit absorption edges at ~ 280 and 370 nm, respectively. The absorption edge of MgO NPs is considerably higher than that of a bulk MgO (~170 nm) due to bulk excitonic transitions for single crystals of MgO [17]. The bandgap of pure MgO NPs and MgO in RHS-MFI is calculated based on the equation $\alpha=A(h\nu-E_g)^{1/2}/h\nu$ where α, E_g and A are the absorption coefficient, bandgap and constant respectively. The evaluated optical band gap energy of pure MgO NPs and in support is 4.42 and 3.35 eV, respectively, and agrees well with values obtained in other works [16]. The observed bandgap value for MgO in nanocomposite showed red-shifted from the pure MgO NPs [17]. The red-shift of the direct band gaps can be attributed to the effect of the morphologies of crystals having various main active sites and or may be due to the quantum size effect.

The valence band (VB) edge position of MgO in MgO/RHS-MFI NC was estimated according to the concept of electronegativity [18]. The conduction band (CB) and VB potentials of the semiconductors at zero point charge could be calculated by the following equation:

$$E_{VB} = X - E^c + 0.5E_g \quad (1)$$

$$E_{CB} = E_{VB} - E_g \quad (2)$$

Where X is the absolute electronegativity of the semiconductors, which is defined as the geometric mean of the constituent atoms absolute electronegativity; Ec the energy of free electrons on the hydrogen scale (ca. 4.5 eV); EVB the VB edge potential and Eg is the bandgap of the semiconductor. The CB position could be deduced from the equation $E_{CB}=E_{VB}-E_g$. The X, E_g, E_{CB}, and E_{VB} values for MgO are calculated 5.68, 3.35, -0.49, and 2.86 eV, respectively. All results indicated that MB degradation could be performed under UV light.

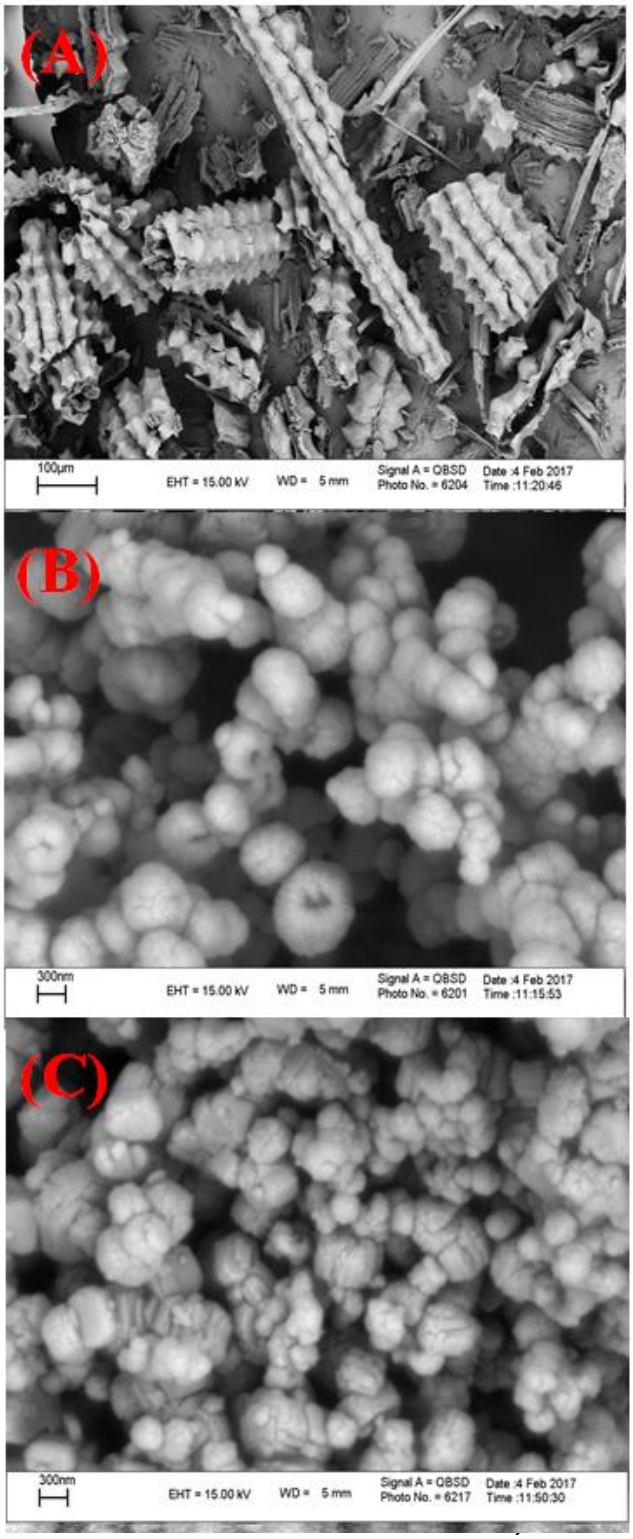

Fig. 2. SEM images of (A) RHS, (B) RHS-MFI and (C) MgO/ RHS-MFI

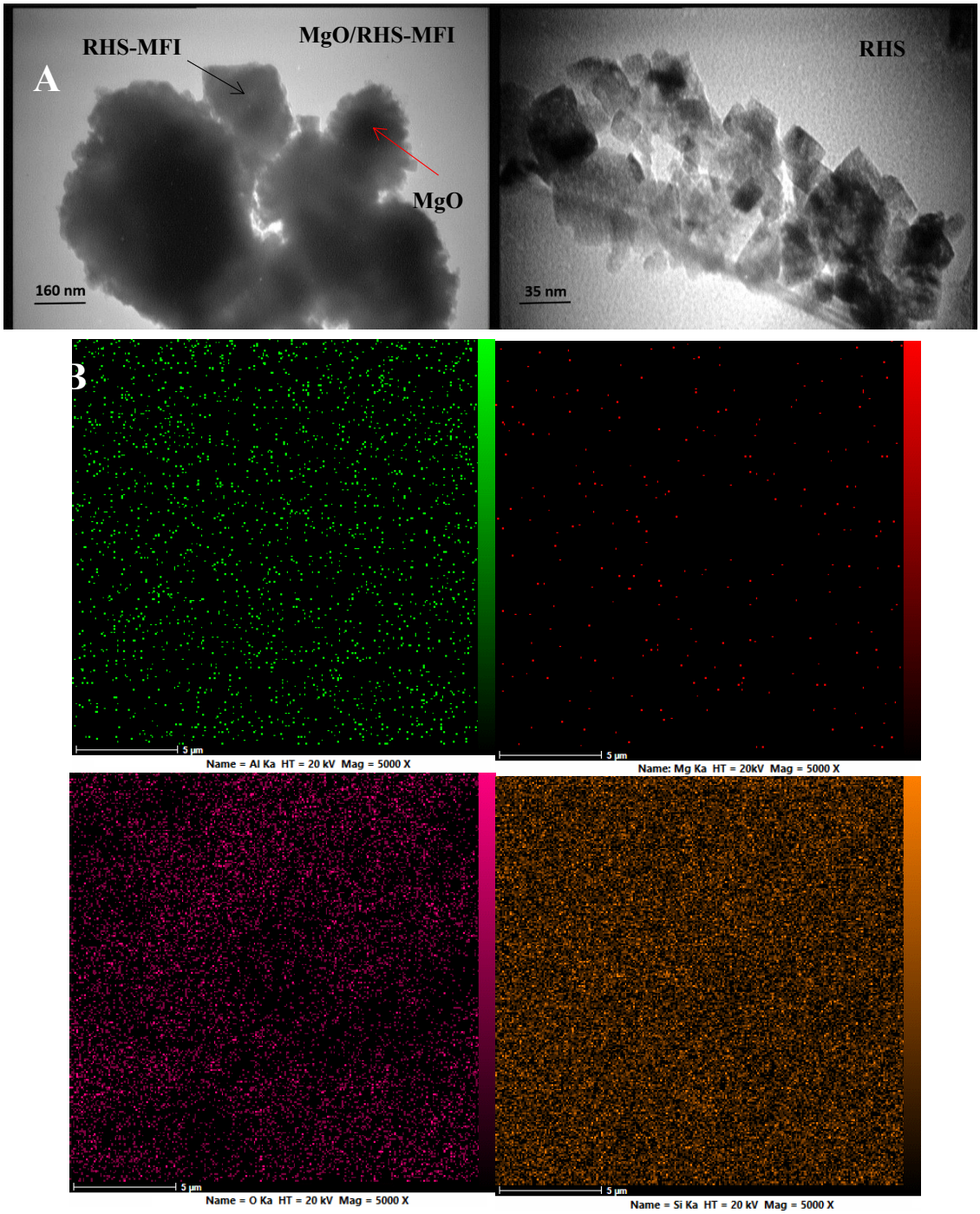

Fig. 3. (A) TEM images of samples and (B) Elemental mapping of MgO/RHS-MFI sample

To follow the undergone changes into the samples' textural evolution, N_2 adsorption-desorption isotherms were measured at −196 °C over calcined samples prepared at different synthesis times. Fig. 5 shows the nitrogen isotherms of RHS-MFI and MgO/RHS-MFI samples. The isotherms corresponding to RHS-MFI indicate a large amount of nitrogen adsorption at high P/P0 that relates to the remaining RHS. The adsorption isotherm of MgO/RHS-MFI reveals

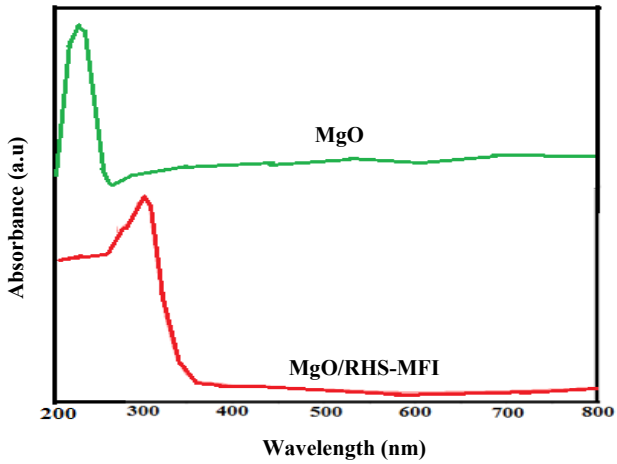

Fig. 4. Diffuse reflectance spectrum of the samples

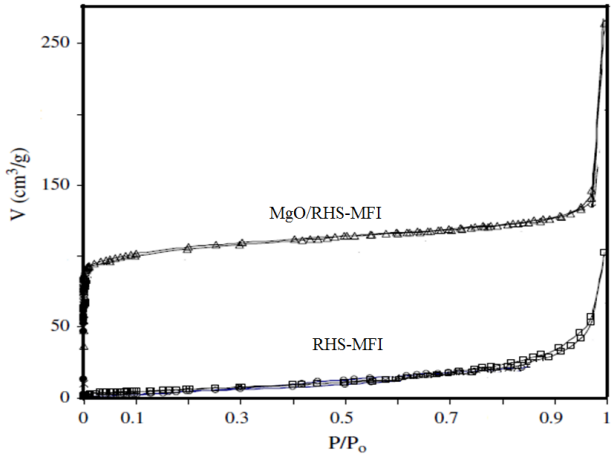

Fig. 5. Nitrogen adsorption-desorption isotherms of samples

the microporosity characteristics of the resulting samples since they consist of sharp knees at P/P0 lower than 0.1 due to the filling of microporous. By nitrogen adsorption/desorption analysis, the RHS-MFI and MgO/RHS-MFI samples indicated a BET surface area of 320 and 270 $m^2 g^{-1}$, respectively. The decreasing of nanocomposite surface area could be related to incorporate MgO NPs into the pore of RHS-MFI.

Photocatalytic activity evaluation

The photocatalytic activity of MgO/RHS-MFI photocatalyst (0.09 g/L) for MB (20 ppm) was tested under UV light irradiation. The reaction pH was controlled at 9 for 60 mins. The photocatalytic performance of the synthesized photocatalysts was calculated in λ = 664 nm of MB dye. The self-degradation of MB in the absence of photocatalyst was insignificant. The removal percent curves of MB dye in the presence of RHS-MFI, MgO NPs, and MgO/RHS-MFI NC are shown in Fig. 6A. The direct UV light photolysis demonstrated in about 5% degradation with no degradation in the absence of MgO/RHS-MFI photocatalyst. About 7 and 30 % of degradation was observed for MB dye in the presence of RHS-MFI and MgO NPs. As shown in Fig. 6A, the synthesized MgO/RHS-MFI photocatalyst indicated ~ 80%, the degradation of MB dye at pH 9 after 60 mins. The MgO NPs and RHS-MFI demonstrated low and high surface area (320 $m^2 g^{-1}$), respectively. Based on the lowest and the highest adsorption was observed for them. It is clear, which the support without semiconductors could not be able to degrade dye. The presence of MgO semiconductor in RHS-MFI support increased MB degradation rate (~80 %). Although,

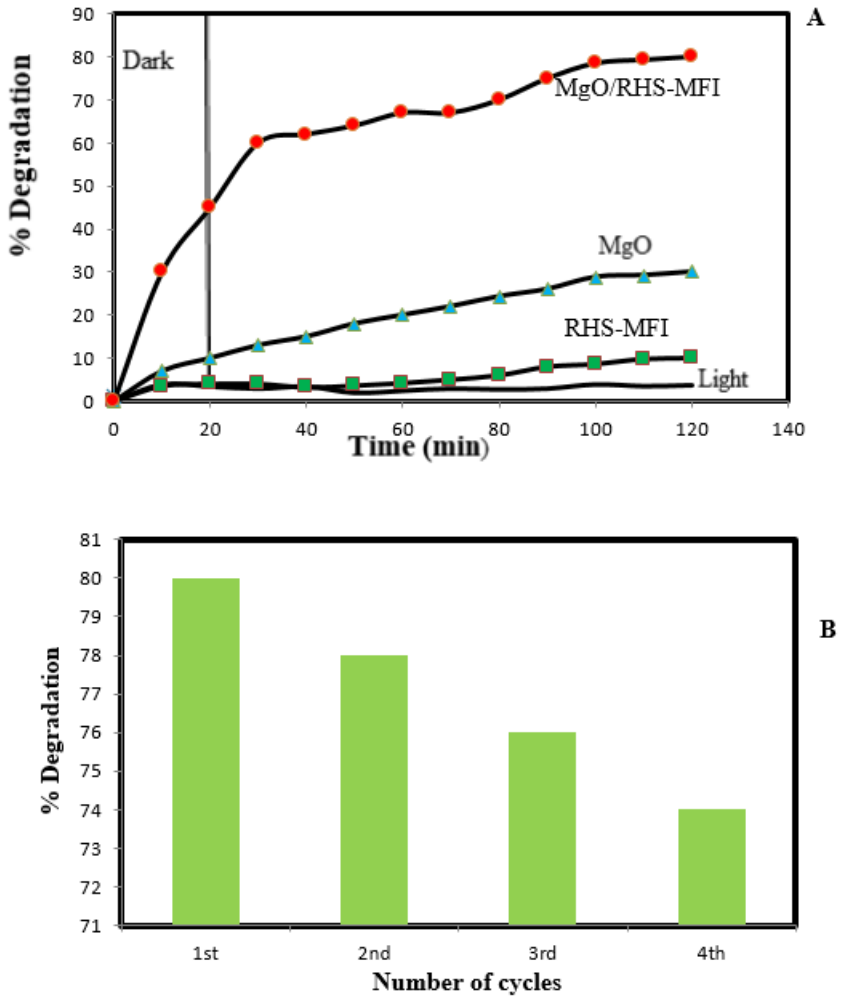

Fig. 6. (A) Degradation percent of different photocatalysts for MB aqueous solution and (B) the cycling degradation efficiency of MB solution in the presence of MgO/RHS-MFI photocatalyst

the existence of Al atoms in the structure of RHS-MFI could influence the degradation performance of MB dye.

In the photocatalytic process, MgO semiconductor produces electron-holes under irradiating photons. Due to the existence of Al atoms in RHS-MFI support, electrons are transferred from the conduction band of MgO to the Al atoms in RHS-MFI. This results in the reduction of electron-hole recombination in MgO and the increment of dye photodegradation. The Electrons from RHS-MFI could be captured by the adsorbed O_2, resulting in the formation of highly reactive hydroxyl radicals ($^{\bullet}OH$) or ($\cdot O_2^-$) for the degradation of organic pollutants.

A prolonged and repeated use of photocatalysts enhances the applicability of MgO/RHS-MFI photocatalyst in wastewater. This further enables the stability of the photocatalyst. Therefore, repeated use of MgO/RHS-MFI was carried out at least for 4 cycles of photocatalytic operations, and the results were illustrated in Fig. 6B. The initial concentration of MB and pH was kept constant. Fig. 6B clearly showed that even after the completion of 4 repeated cycles, the percentage efficiency of MB photocatalytic degradation was not suppressed and almost constant photocatalytic degradation was obtained. XRD patterns of MgO/RH-MFI after the photocatalyst process are shown in Fig. 7A. You can see there is very little difference between the first and reused sample. More quantitatively, after 4 cycles, the percentage removal of MB dye was decreased from 80 % to 74% only (i.e., a decrease of 6%). The results indicated that the new

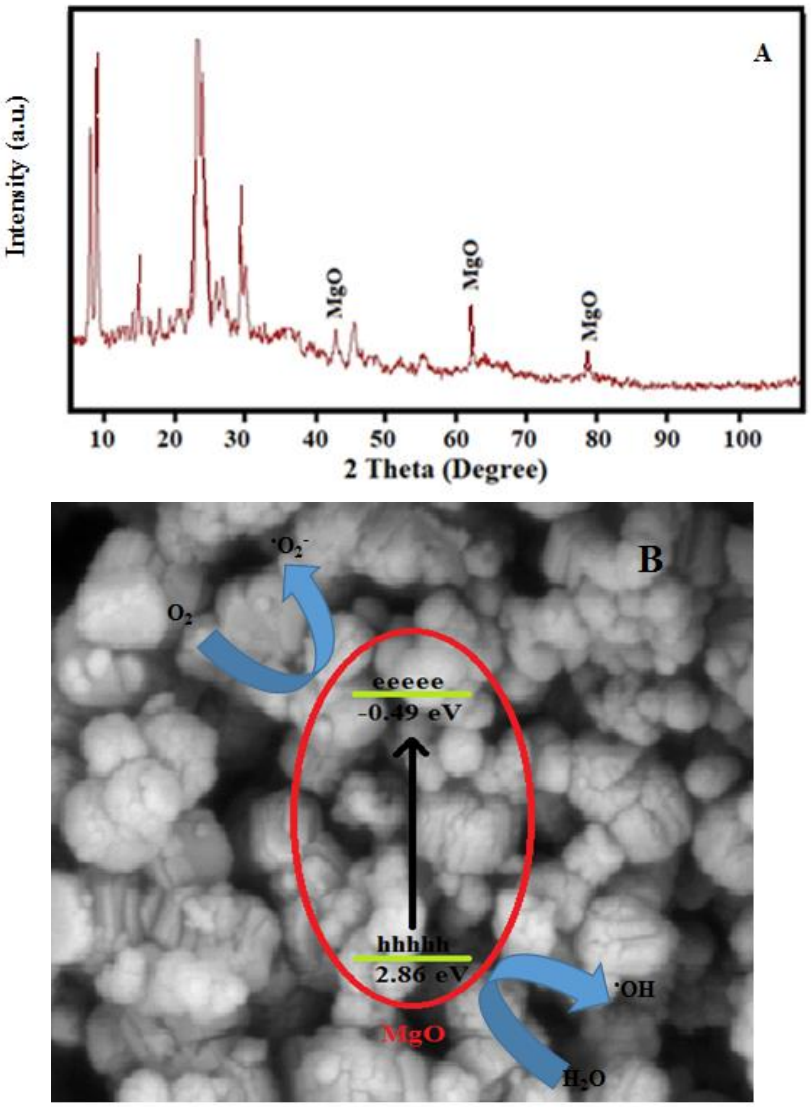

Fig. 7. (A) XRD patterns of MgO/RHS-MFI after irradiation UV-light in photocatalyst process and (B) Schematic illustration for the proposed mechanism of photocatalytic degradation of MB by MgO/RHS-MFI nanocomposites

photocatalyst was found to be fairly stable at least for the repeated photocatalytic degradation of MB from aqueous solutions. This eventually enhances the applicability of the photocatalyst in several wastewater treatment strategies and even could provide a greener treatment option.

Reaction mechanism

The MgO semiconductor possessed a wide bandgap of 4.42 eV [16]. Absorption of UV light lifts electrons from the valance band (VB) to the conduction band (CB) that leaves behind a hole in the VB; therefore, the photogenerated electron/hole (e-/h+) pairs stimulate the reduction and oxidation processes onto the surface of the photocatalysts. Later on, in the presence of water and oxygen, radical species such as $^{\bullet}OH$, H_2O_2, or $^{\bullet}O_2^-$ are produced. These radical species attack the organic molecule adsorbed on the catalyst surface. This, therefore, results in cleavage of bonds within the organic molecule; hence, the degradation of organic pollutants takes place in an aqueous medium on the catalyst surface. The scheme of a possible photocatalytic mechanism is presented in Fig. 7B. Based on the obtained DRS results, E_{V_B} E_{V_B} and $E_{C_B}E_{C_B}$ were calculated 2.86 and -0.49 eV, respectively.

The first hypothesis in the case of the

Table 1. The photogenerated active species trapped in the system of photodegradation of MB by MgO/RHS-MFI photocatalyst under visible light irradiation

samples	*IPA(•OH)*	*BQ (•O_2^-)*	*CAT (H_2O_2)*	*EDTA (h^+)*	No scavenger
%D MgO/RHS-MFI	20.0	28.0	74.0	25.0	80.0

photodegradation mechanism could be related to the excited electrons from the V_B to the C_B position for MgO semiconductor under UV light irradiation. The electrons on the C_B of MgO could be transferred to O_2 molecules in solution and generate $^{\bullet}O_2^-$ on the photocatalyst surface [19]. The V_B potential of MgO (holes) (2.86 eV) which is more positive than the oxidation reaction of H_2O (E^0 ($H_2O/^{\bullet}OH$) (2.72 eV vs SHE), could produce $^{\bullet}OH$ by the oxidation of H_2O with holes [20]. Therefore, the mechanism of photodegradation could be expressed as follows:

$$MgO + h\nu \rightarrow MgO\ (e^- + h^+) \quad (3)$$

$$MgO\ (e) + O_2 \rightarrow {}^{\bullet}O_2^- \quad (4)$$

$$MgO\ (h^+) + H_2O \rightarrow {}^{\bullet}OH \quad (5)$$

$$^{\bullet}OH/^{\bullet}O_2^- + MB \rightarrow \text{degradation products} \quad (6)$$

In the secondary hypothesis, electrons in the C_B position of MgO semiconductor could be entered into pores of RHS-MFI micropore support or accepted by Al atoms of MFI zeolite. Subsequently, electrons act as centers for two-electron reduction process of O_2 to form H_2O_2 or $^{\bullet}OH$. The holes in the V_B of MgO react with H_2O to produce active $^{\bullet}OH$. The $^{\bullet}OH$ could convert MB to CO_2 and H_2O. The photodegradation mechanism is:

$$MgO/RHS\text{-}MFI + h\nu \rightarrow MgO\ (e^- + h^+)/RHS\text{-}MFI \quad (7)$$

$$MgO\ )e^-_{CB}) + RHS\text{-}MFI \rightarrow MgO + RHS\text{-}MFI\ (e) \quad (8)$$

$$RHS\text{-}MFI\ (2e^-) + O_2 + 2H^+ \rightarrow H_2O_2 \quad E^{\circ} = +0.68 \quad (9)$$

$$H_2O_2 + e^- \rightarrow OH^- + {}^{\bullet}OH \quad E^{\circ} = +0.38 \quad (10)$$

$$MgO\ (h^+) + H_2O \rightarrow H^+ + {}^{\bullet}OH \quad E^{\circ} = +2.27 \quad (11)$$

$$^{\bullet}OH + h^+ + MB \rightarrow \text{Products} \quad (12)$$

The presence of radical scavengers such as Isopropyl alcohol (IPA) was reported to be a good scavenger of $^{\bullet}OH$ radicals [21]. Similarly, the benzoquinone (BQ), Catalase, and EDTA have scavenged significantly the $^{\bullet}O_2^-$, H_2O_2, and h^+ photocatalyst [22] and sodium azide (NaN_3) that could suppress the singlet oxygen which is produced by the interaction of superoxide radical and photogenerated holes. Therefore, the photocatalytic degradation of MB dye in the presence of BQ, catalase, IPA, and EDTA was carried out using the MgO/RHS-MFI photocatalyst. The results are shown in Table 1. Table 1 clearly showed that in the presence of IPA, BQ, and EDTA a significant decrease in the percentage removal of MB dye was observed, or in other words, these scavengers significantly inhibited the removal of MB in the photocatalytic degradation. This, therefore, confirmed the $^{\bullet}OH$, $^{\bullet}O_2^-$, and hole radicals were predominantly involved in the photocatalytic degradation of MB.

CONCLUSION

In summary, MgO nanoparticles were incorporated in RHS-MFI zeolite using a solid-state method. The formation of MgO nanoparticles in zeolite was observed by TEM, SEM, XRD, BET, and DRS. The synthesized zeolite was used in the degradation of MB dye under UV-light. RHS-MFI zeolite had an important role in the increase of MB dye absorption over the photocatalyst and the separation of MgO NPs electron-hole. Results indicated that MgO/ RHS-MFI photocatalyst increased the percentage of MBs degradation to 80.0 %. The degradation of MB in the presence of scavengers demonstrated that $^{\bullet}OH$, $^{\bullet}O_2^-$, and H^+ as reactive species play the main role in the photocatalytic oxidation process. Based on the obtained experimental results, MgO/RHS-MFI as an efficient, stable, and effective catalyst could be used effectively for UV photocatalytic oxidation. This work is expected to show a new direction for MB-based nanocomposite investigation and potential applications.

ACKNOWLEDGEMENTS

The authors are grateful to the Islamic Azad University, Rasht Branch.

CONFLICT OF INTEREST

The authors declare no conflict of interest.

REFERENCES

1. Mittal H, Maity A, Ray SS. Synthesis of co-polymer-grafted gum karaya and silica hybrid organic–inorganic hydrogel nanocomposite for the highly effective removal of methylene blue. Chemical Engineering Journal. 2015;279:166-79.

2. Oladipo AA, Gazi M, Saber-Samandari S. Adsorption of anthraquinone dye onto eco-friendly semi-IPN biocomposite hydrogel: Equilibrium isotherms, kinetic studies and optimization. Journal of the Taiwan Institute of Chemical Engineers. 2014;45(2):653-64.
3. Pourahmad A. Fabrication of Nanocatalyst in Aqueous Solution With Photocatalytic Activity of Methylene Blue. Synthesis and Reactivity in Inorganic, Metal-Organic, and Nano-Metal Chemistry. 2015;45(7):1080-6.
4. Alvarado E, Torres-Martinez LM, Fuentes AF, Quintana P. Preparation and characterization of MgO powders obtained from different magnesium salts and the mineral dolomite. Polyhedron. 2000;19(22-23):2345-51.
5. Wang W, Qiao X, Chen J. The Role of Acetic Acid in Magnesium Oxide Preparation via Chemical Precipitation. Journal of the American Ceramic Society. 2008;91(5):1697-9.
6. Ahmadpour N, Sayadi MH, Sobhani S, Hajiani M. A potential natural solar light active photocatalyst using magnetic ZnFe2O4 @ TiO2/Cu nanocomposite as a high performance and recyclable platform for degradation of naproxen from aqueous solution. Journal of Cleaner Production. 2020;268:122023.
7. Sayadi MH, Sobhani S, Shekari H. Photocatalytic degradation of azithromycin using GO@Fe3O4/ ZnO/ SnO2 nanocomposites. Journal of Cleaner Production. 2019;232:127-36.
8. Singh P, Sharma K, Hasija V, Sharma V, Sharma S, Raizada P, et al. Systematic review on applicability of magnetic iron oxides–integrated photocatalysts for degradation of organic pollutants in water. Materials Today Chemistry. 2019;14:100186.
9. Gholami A, Hajiani M, Sayadi Anari M H. Investigation of Photocatalytic Degradation of Clindamycin by TiO_2. Journal of Water and Environmental Nanotechnology. 2019; 4(2):139-146.
10. Venkatesha TG, Viswanatha R, Arthoba Nayaka Y, Chethana BK. Kinetics and thermodynamics of reactive and vat dyes adsorption on MgO nanoparticles. Chemical Engineering Journal. 2012;198-199:1-10.
11. Sun Q, Hu X, Zheng S, Sun Z, Liu S, Li H. Influence of calcination temperature on the structural, adsorption and photocatalytic properties of TiO2 nanoparticles supported on natural zeolite. Powder Technology. 2015;274:88-97.
12. Kordatos K, Ntziouni A, Iliadis L, Kasselouri-Rigopoulou V. Utilization of amorphous rice husk ash for the synthesis of ZSM-5 zeolite under low temperature. Journal of Material Cycles and Waste Management. 2013;15(4):571-80.
13. Jorfi S, Barzegar G, Ahmadi M, Darvishi Cheshmeh Soltani R, alah Jafarzadeh Haghighifard N, Takdastan A, et al. Enhanced coagulation-photocatalytic treatment of Acid red 73 dye and real textile wastewater using UVA/ synthesized MgO nanoparticles. Journal of Environmental Management. 2016;177:111-8.
14. Ziksari M, Pourahmad A. Green synthesis of CuO/ RHA-MCM-41 nanocomposite by solid state reaction: Characterization and antibacterial activity. Indian Journal of Chemistry -Section A. 2016;55A:1347-1351.
15. Sohrabnezhad S, Pourahmad A, Zanjanchi MA. Incorporation of CoS nanoparticles into ZSM-5 zeolite by hydrothermal and ion exchange methods. Journal of the Iranian Chemical Society. 2009;6(3):612-9.
16. Bindhu MR, Umadevi M, Kavin Micheal M, Arasu MV, Abdullah Al-Dhabi N. Structural, morphological and optical properties of MgO nanoparticles for antibacterial applications. Materials Letters. 2016;166:19-22.
17. Williams MW, Arakawa ET. Optical Properties of Single-Crystal Magnesium Oxide. Journal of Applied Physics. 1967;38(13):5272-6.
18. Yu H, Xu L, Wang P, Wang X, Yu J. Enhanced photoinduced stability and photocatalytic activity of AgBr photocatalyst by surface modification of Fe(III) cocatalyst. Applied Catalysis B: Environmental. 2014;144:75-82.
19. Ye L, Chen J, Tian L, Liu J, Peng T, Deng K, et al. BiOI thin film via chemical vapor transport: Photocatalytic activity, durability, selectivity and mechanism. Applied Catalysis B: Environmental. 2013;130-131:1-7.
20. Asadollahi A, Sohrabnezhad S, Ansari R. Enhancement of photocatalytic activity and stability of Ag2CO3 by formation of AgBr/Ag2CO3 heterojunction in mordenite zeolite. Advanced Powder Technology. 2017;28(1):304-13.
21. Zhang L-S, Wong K-H, Yip H-Y, Hu C, Yu JC, Chan C-Y, et al. Effective Photocatalytic Disinfection ofE. coliK-12 Using AgBr−Ag−Bi2WO6Nanojunction System Irradiated by Visible Light: The Role of Diffusing Hydroxyl Radicals. Environmental Science & Technology. 2010;44(4):1392-8.
22. Li G, Wong KH, Zhang X, Hu C, Yu JC, Chan RCY, et al. Degradation of Acid Orange 7 using magnetic AgBr under visible light: The roles of oxidizing species. Chemosphere. 2009;76(9):1185-91.